

Laboratory Measurements of Differential Diffusion in a Diffusively Stable, Turbulent Flow

P. RYAN JACKSON AND CHRIS R. REHMANN

Hydrosystems Laboratory, Department of Civil and Environmental Engineering, University of Illinois at Urbana–Champaign, Urbana, Illinois

(Manuscript received 10 April 2002, in final form 19 February 2003)

ABSTRACT

Laboratory experiments were performed to determine the conditions under which differential diffusion occurs and to evaluate its effect on the mixing efficiency. Diffusively stable profiles of temperature and salinity were stirred steadily by horizontally oscillating vertical rods. The two-component stratification ensures that both scalars experience the same stratification and forcing, or Richardson and Reynolds numbers. The eddy diffusivities K_T and K_S , for temperature and salinity, were estimated by fitting theoretical solutions of diffusion equations to measured profiles, and the mixing efficiency was computed as the ratio of the potential energy change during a stirring interval to the work done in that interval. Differential diffusion occurred for $\varepsilon_a/\nu N^2 < 300\text{--}500$, where ε_a is an average dissipation rate computed from an integrated energy budget. The diffusivity ratio $d = K_S/K_T$ varied between 0.5 and 1 in the range $50 < \varepsilon_a/\nu N^2 < 500$. The experiments also show that differential diffusion can significantly affect the mixing efficiency. An important dimensionless parameter is the density ratio R_ρ , which is the ratio of the density change due to temperature to that due to salinity. Measurements in cases with low density ratio ($R_\rho \approx 0.25$) and high density ratio ($R_\rho \approx 5$) showed that the mixing efficiencies agreed well for weak stratification, or small Richardson number. For larger Richardson number, the efficiency for the high-density-ratio case exceeded that for the low-density-ratio case by as much as a factor of 1.5.

1. Introduction

Oceanographers often assume that active scalars like salt S and temperature T mix at equal rates in a diffusively stable, turbulent flow. For example, in turbulence models like those used in general circulation models, the eddy diffusivities K_S and K_T of salt and temperature are frequently taken to be equal. Also, in most studies of ocean microstructure the eddy diffusivity for temperature estimated with the Osborn–Cox model (Osborn and Cox 1972) is assumed to be equal to the eddy diffusivity for density estimated with the Osborn (1980) model. However, the eddy diffusivities could differ if the transport of scalars in the ocean depends on the molecular diffusivity D of the different scalars. Since the Schmidt number $Sc = \nu/D$ of 700 for saltwater is one hundred times greater than that for heated water, molecular diffusion may affect the mixing when the large, energy-containing eddies are not much larger than the dissipating eddies. In these cases differential diffusion, or differential transport of salt and heat, can

occur. In this paper we use laboratory experiments to identify conditions for differential diffusion.

Evidence for differential transport of heat and salt comes from laboratory experiments, numerical computations, and field observations (Gargett 2003). Turner (1968) and Altman and Gargett (1990) found that the entrainment of heat across a density interface exceeded the entrainment of salt when the stratification was strong, or when a Richardson number based on the density jump and scales of the turbulence was large. Because the eddy diffusivity is proportional to the entrainment rate, or flux, across the density interface (Linden 1979), Turner's measurements can be used to show that the diffusivity ratio $d = K_S/K_T$ was between 0.3 and 1 (e.g., Gargett and Holloway 1992; Gargett and Ferron 1996). Similarly, numerical simulations of two-dimensional turbulence show greater transport of heat than salt for weak turbulence in a strongly stratified fluid (Merryfield et al. 1998). Recent field measurements by Nash and Moum (2002) on the Oregon continental shelf yield a mean value of d of about 0.7.

The conditions for differential diffusion are still uncertain, however. If u and L_T are the velocity and length scales of the large eddies and N is the buoyancy frequency, then effects of molecular diffusion should appear when both the Froude number $Fr_T = u/NL_T$ and the Reynolds number $Re_T = uL_T/\nu$ are small. In terms

Corresponding author address: C. R. Rehmann, Department of Civil and Environmental Engineering, University of Illinois at Urbana–Champaign, 2527 Hydrosystems Laboratory, 205 N. Mathews Ave., Urbana, IL 61801.
E-mail: rehmann@uiuc.edu

of the parameter $\varepsilon/\nu N^2$, used frequently in oceanographic studies, molecular diffusion should be important when $\varepsilon/\nu N^2$ is small. Field measurements of Nash and Moum (2002) over about four decades of $\varepsilon/\nu N^2$ show values of $d < 1$, but because of measurement uncertainty, Nash and Moum (2002) could not rule out $d \approx 1$. Nash and Moum (2002) also cast Turner's (1968) laboratory measurements of entrainment in the form of d versus $\varepsilon/\nu N^2$ to show that differential diffusion occurs for $\varepsilon/\nu N^2 < 100$, at least for two-layer entrainment experiments. In other laboratory experiments, Nagata and Komori (2001) found a difference in eddy diffusivities for active heat and a passive scalar in weakly and strongly stratified cases, though the difference was more pronounced when the stratification was strong. Towed-grid experiments of Rehmann and Koseff (2003, submitted to *Dyn. Atmos. Oceans*, hereinafter RK) over a wide range of Richardson number based on grid scales showed no difference between mixing efficiencies for temperature-stratified and salt-stratified water. However, at a fixed Richardson number the Reynolds number for the temperature-stratified case was lower than that for the corresponding salt-stratified case. To subject both scalars to the same stratification and forcing, they suggested performing experiments in which a two-component, stable stratification is mixed.

Differential diffusion can affect the prediction and interpretation of vertical mixing in the ocean. Using the Geophysical Fluid Dynamics Laboratory circulation model, Gargett and Holloway (1992) found that slight differences in the eddy diffusivities can produce large differences in the predicted thermohaline circulation, though effects of differential diffusion are much smaller in a global ocean model (Merryfield et al. 1999). Gargett and Ferron (1996) studied the effects of differential diffusion with a diffusive box model and concluded that further study of differential diffusion is required to improve the predictions of ocean models. Differential diffusion can also affect eddy diffusivities estimated from microstructure measurements. Differences between K_T and K_ρ are usually attributed to variations in the mixing efficiency (e.g., Oakey 1982), which depends on the strength of the stratification and the process generating the turbulence (Linden 1979; Ivey and Imberger 1991). When differential diffusion occurs, the relative contributions of temperature and salinity to the density will be important also; the relevant dimensionless parameter is the density ratio $R_\rho = \alpha\Delta T/\beta\Delta S$, where ΔT and ΔS are the magnitudes of the temperature and salinity difference and α and β are the thermal expansion and saline contraction coefficients, respectively.¹ If $K_T > K_S$, then in cases with larger density ratio the fluid's potential energy will change more quickly, or the mixing efficiency will be greater. Jackson and Rehmann (2003)

showed that differential diffusion can produce significant changes in the mixing efficiency and affect the production of layering or finestructure.

We use laboratory experiments to determine the conditions under which differential diffusion occurs and its effect on the mixing efficiency in a diffusively stable, turbulent flow. A tank is stratified with both salt and heat and stirred steadily with oscillating rods. Eddy diffusivities and mixing efficiency are determined from changes in temperature and salinity profiles and force measurements during stirring. Merits of the experiments include the steadiness of the stirring, the direct measurement of eddy diffusivities and work input, and the two-component stratification. Steady forcing removes complications of changing turbulent scales and facilitates the interpretation of the results. Computing the eddy diffusivities from the scalar profiles and the rate of work input from force measurements avoids uncertainty due to assumptions in the indirect microstructure methods. The two-component stratification ensures that both scalars experience the same stratification and forcing, or Froude and Richardson numbers. In section 2 we describe the experimental facility and procedures. We discuss the results in section 3 and summarize in section 4.

2. Experimental procedures and uncertainty

Each experiment started by stratifying a tank with linear, diffusively stable profiles of both temperature and salinity. Initial temperature and salinity profiles were measured with a temperature–conductivity probe, and the fluid was stirred with oscillating vertical rods for approximately 30 minutes. During the stirring the drag on one of the rods was measured so that the work done by the rods on the fluid could be estimated. After the stirring was stopped, the motions were allowed to decay for a sufficient period, and profiles were measured again. The stirring and profiling was repeated until the change in potential energy was at least half of the maximum possible change. The mixing efficiency was calculated as the ratio of the change in mean potential energy to the work done, and eddy diffusivities of heat, salt, and density were also computed. Experimental parameters are shown in Table 1.

The experimental facility was 2 m long, 0.4 m wide, and 0.6 m deep (Fig. 1), and the temperature and salinity profiles were established with the double-bucket method of Fortuin (1960). Care was taken to minimize heat losses. The bottom and sidewalls consisted of foam sandwiched between fiberglass-reinforced plastic with a small Plexiglas window for viewing. A combination of a Plexiglas cover and Styrofoam insulated the area just above the water surface. An additional 4 cm of insulation was also added to the tank exterior. A 4-cm-thick layer of Styrofoam beads with a mean diameter of approximately 1 cm on the water surface further re-

¹ The density ratio defined in this way is positive. If the definition from salt fingering studies were used, the density ratio would have the same magnitude, but it would be negative.

TABLE 1. Experimental parameters. For all runs, the stroke S was 7.5 cm and the depth H was 50 cm. Values for stratification parameters are initial values. Both the Froude and Reynolds numbers are defined using estimates of turbulence scales. The length scale L_T is taken to be the spacing between the combs, and the velocity scale is estimated as $(\epsilon_r L_T)^{1/3}$.

Expt	ω (rad s ⁻¹)	Fr_T	Re_T	Ri_T	R_p	N (rad s ⁻¹)	$\epsilon_r/\nu N^2$
6	0.97	0.97	706	1.07	5.18	0.30	663
7	0.97	1.02	526	0.96	0.28	0.29	550
8	0.47	0.47	287	4.51	0.29	0.34	64
9	0.47	0.46	399	4.68	5.41	0.34	85
10	2.13	2.31	1220	0.19	0.29	0.29	6510
11	2.13	2.37	1810	0.18	4.88	0.30	10 100
12	0.61	0.60	503	2.81	5.94	0.33	179
13	0.63	0.54	380	3.46	0.28	0.38	110

duced heat losses without interfering with the stirring rods.

Experiments were performed to quantify the heat losses through both the water surface and the sidewalls of the tank. The experiments were conducted in a manner similar to that of Muñoz and Zangrando (1986) in which the tank was filled with water of uniform temperature and allowed to sit. Temperature profiles were recorded every 10 minutes for approximately 6 to 8 hours. By performing several experiments with and without extra surface insulation, the losses through the surface and the losses through the sidewalls were isolated. From an energy balance, heat loss coefficients for the tank sidewalls and water surface were determined. These calculations showed that the addition of the Styrofoam beads reduced the surface heat loss coefficient by a factor of 10. Remaining surface heat losses were included in the diffusivity calculations by including a flux boundary condition at the surface, as described later in this section. The sidewall heat loss coefficient was 1.2 W/(m²K); this value was used to compute the net sidewall heat flux differential, or the difference between

the fluxes through the upper half and the lower half of the tank.

Turbulence was generated with a stirring mechanism similar to that used by Ruddick et al. (1989). Combs of vertical rods oscillated horizontally along the length of the tank with a stroke of 7.5 cm and frequencies between 0.1 and 0.34 Hz. On each comb, 1.27 cm × 1.27 cm fiberglass rods were mounted 15 cm apart. Ten combs were mounted at equal spacing (4 cm on center) across the width of the tank. To reduce mean flows, neighboring combs oscillated 180° out of phase. Computer control of the stepper motor driver mechanism maintained constant stirring throughout the experiments. Thirty-minute intervals of stirring were followed by approximately 12 minutes of waiting for turbulence and internal waves to decay before profiles were measured.

The work done on the fluid was estimated from direct measurements of the drag on one of the rods. A Futek Technologies moment load cell was mounted along one of the stirring rods. Because the rod fitted with the load cell had a span of reduced cross sectional area at the load cell, it had a small vibration at a frequency (~8 Hz) much higher than the stirring frequency. The drag record was filtered to remove the high-frequency oscillations since visual observations confirmed the lack of such vibrations in the other rods. The resulting drag compared well with that computed from a theory of square rods oscillating in an otherwise stationary fluid (Sumer and Fredsøe 1997). The work done by the gauged rod was calculated by integrating the product of the drag and the rod velocity, which was monitored with a tachometer, and the total work done by all of the rods was computed by assuming that the other rods behave similarly.

Temperature and conductivity profiles were measured with a Precision Measurements Engineering Model 125 MicroScale Conductivity–Temperature Instrument (MSCTI), which consists of a Thermometrics FP07

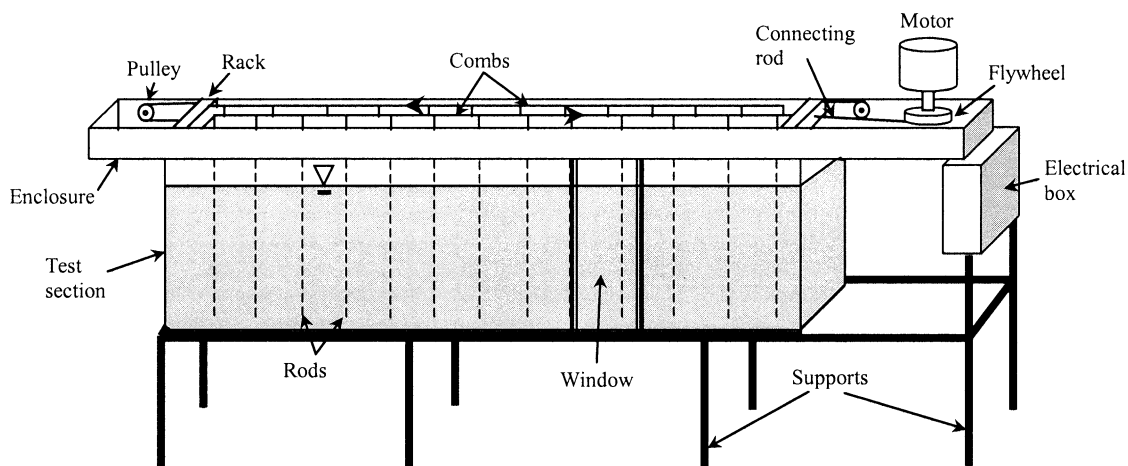


FIG. 1. Schematic of the experimental facility. The fluid is stirred by horizontally oscillated “combs” of vertical rods. Neighboring combs oscillate 180° out of phase. Only 2 of 10 comb sets are shown for simplicity.

thermistor mounted approximately 1 mm from a four-electrode conductivity sensor (Head 1983). The thermistor was calibrated using a Thermometrics high-resolution digital thermometer with 0.002°C accuracy, and the conductivity sensor was calibrated using five solutions of known salinity. Profiles were measured at four equally spaced locations along the tank centerline. The MSCTI traversed the region from about 10 mm below the water surface to 5 mm above the tank bottom at 10 cm s⁻¹, and its vertical position was computed from the probe speed and the elapsed travel time. A digital trigger ensured that data acquisition started when the MSCTI began moving. The profiles were filtered and extrapolated to the boundaries (Park et al. 1994; RK) before density was computed.

Eddy diffusivities for temperature and salinity were computed by fitting theoretical solutions to the diffusion equation to the measured profiles. For salinity, the eddy diffusivity K_s was taken as the value that minimized the sum of the squared differences between the measured profiles and theoretical profiles computed with no-flux boundary conditions. For temperature, a flux boundary condition was imposed at the surface to account for heat losses, and optimal values of the heat loss coefficient and eddy diffusivity K_T were found. For each experiment, eddy diffusivities were determined for sequential pairs of profiles, and periods of molecular diffusion were included to simulate the waiting interval between the end of stirring and profiling.

Mixing efficiencies were computed from the density profiles and work measurements. The change in potential energy between two profiles was computed as

$$\Delta PE = gB \int_0^L \int_0^H z(\rho_{n+1} - \rho_n) dz dx, \quad (1)$$

where L , B , and H are the length, width, and depth of the fluid, respectively. For each stirring interval in an experiment, the mixing efficiency was then computed as the ratio of the potential energy change and the work W done on the fluid during the stirring interval:

$$R_f = \frac{\Delta PE}{W}. \quad (2)$$

Eddy diffusivities for density were related to the mixing efficiency by

$$K_\rho = R_f \frac{dW/dt}{\rho_0 LBHN_n^2}, \quad (3)$$

where N_n is the buoyancy frequency computed from the average density gradient during the n th stirring interval (Barry et al. 2001). The rate of work input was computed from a least squares line fit to t versus W .

Errors in the mixing efficiency and eddy diffusivity for density mainly reflect errors in mass conservation, which are due to drift of the conductivity sensor and heat losses that had not been accounted for by the diffusion calculation. Changes in the added mass

$$M_a = LB \int_0^H (\rho - \rho_{s0}) dz, \quad (4)$$

where ρ_{s0} is the initial surface density, were used to assess errors in mass conservation. In the present experiments, the change in added mass was always less than 4% of the initial value. This change corresponds to a change in *total* mass of about 0.01%. For comparison, the experiments of Linden (1980) and Holford and Linden (1999) conserve total mass to 0.02%–0.05%.

The average dissipation rate ε_a of turbulent kinetic energy was computed from an integrated energy budget. For these experiments the rate of work input is equal to the rate of change of potential energy plus the dissipation integrated over the volume:

$$\frac{dW}{dt} = \frac{dPE}{dt} + \int_V \rho_0 \varepsilon dV. \quad (5)$$

Along with the definition of the mixing efficiency, Eq. (5) can be rearranged to estimate the volume-averaged dissipation as

$$\varepsilon_a \equiv \frac{1}{V} \int_V \varepsilon dV = \frac{dW/dt}{\rho_0 V} (1 - R_f). \quad (6)$$

With an estimate of the dissipation from Eq. (6), results can be presented as a function of the parameter $\varepsilon_a/\nu N^2$, which is often used to describe the state of oceanic turbulence.

3. Results and discussion

The evolution of temperature, salinity, and density profiles is discussed first, and evidence for differential diffusion from T - S diagrams is presented. Eddy diffusivities are then presented in several forms; in particular, the diffusivity ratio is shown to identify the conditions under which differential diffusion occurs. Effects of differential diffusion on mixing efficiency are then assessed.

a. Profile evolution

The evolution of the density profiles was similar to that in other experiments with relatively weak stratification (Britter 1985; Rottman and Britter 1986; Barrett and Van Atta 1991). The experimental parameters are listed in Table 1, and the location of the present experiments in the Froude number–Reynolds number plane is depicted in Fig. 2. Experiments were conducted using high and low initial density ratios, though the density ratio evolved slightly over each experiment. Each experiment began with linear, stable profiles of both temperature and salt. Mixed layers formed at the top and the bottom of the tank and extended into the interior as the stirring progressed (Fig. 3). The observed profiles superficially resemble profiles predicted from an eddy diffusion model (Rottman and Britter 1986;

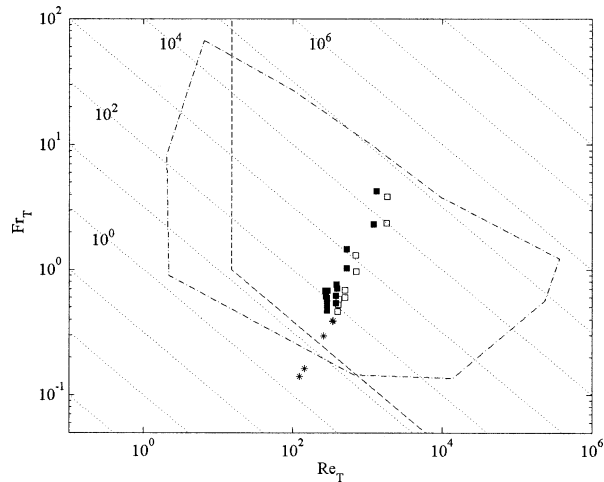


FIG. 2. Location of present experiments in the Froude number–Reynolds number plane of Ivey and Imberger (1991). Filled squares denote experiments with low density ratio ($R_\rho \approx 0.25$) and open squares denotes experiments with high density ratio ($R_\rho \approx 5$). Stars are computed from the experiments of Ruddick et al. (1989). The dash–dot line outlines the region in which the measurements of Imberger and Ivey (1991) fall. Upgradient fluxes occur to the left of the dashed line (Ivey and Imberger 1991). Dotted lines are contours of $\varepsilon/\nu N^2$, spaced by factors of 10.

RK). In cases with stronger stratification, other researchers have observed layered density profiles that form from an initially linear profile (e.g., Ruddick et al. 1989), but Fig. 2 suggests that the stratification was weak enough and the turbulence was strong enough in the present experiments to prevent layer formation.

The evolution of the scalar profiles is shown in the T – S diagrams of Fig. 4. If temperature and salt mix equally during an experiment, then subsequent T – S curves will lie on top of the initial curve, but they will be shortened because the temperature and salinity differences decrease. When differential diffusion occurs, the T – S curve will rotate with respect to the initial curve. For example, Gargett (2003) presented T – S curves from profiles in a tidal channel that are consistent with differential diffusion, although she could not discount other explanations. For our experiments, Figs. 4a and 4b show characteristics of differential diffusion. In both, the T – S curves rotate counterclockwise since temperature mixes faster than salt—that is, $d < 1$. Analytical solutions of eddy diffusion equations for salinity and temperature with constant eddy diffusivities show that in cases with lower d the normalized T – S curves will rotate more during the same time period normalized by H^2/K_T . Because the T – S curves in Fig. 4b rotate more than those in Fig. 4a and the values of K_T for the two experiments are approximately equal, experiment 9 should have a lower d than experiment 8.

b. Eddy diffusivities

Eddy diffusivities for temperature and salinity are shown as a function of the average dissipation in Fig.

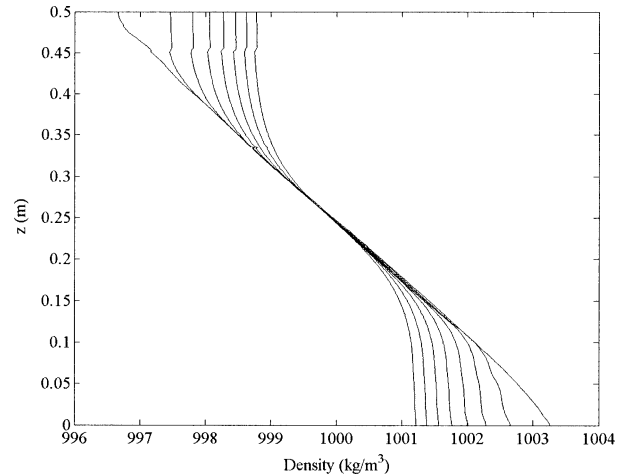


FIG. 3. Typical density profile evolution. The profiles are taken from expt 8. Profiles are separated by 30 min of stirring.

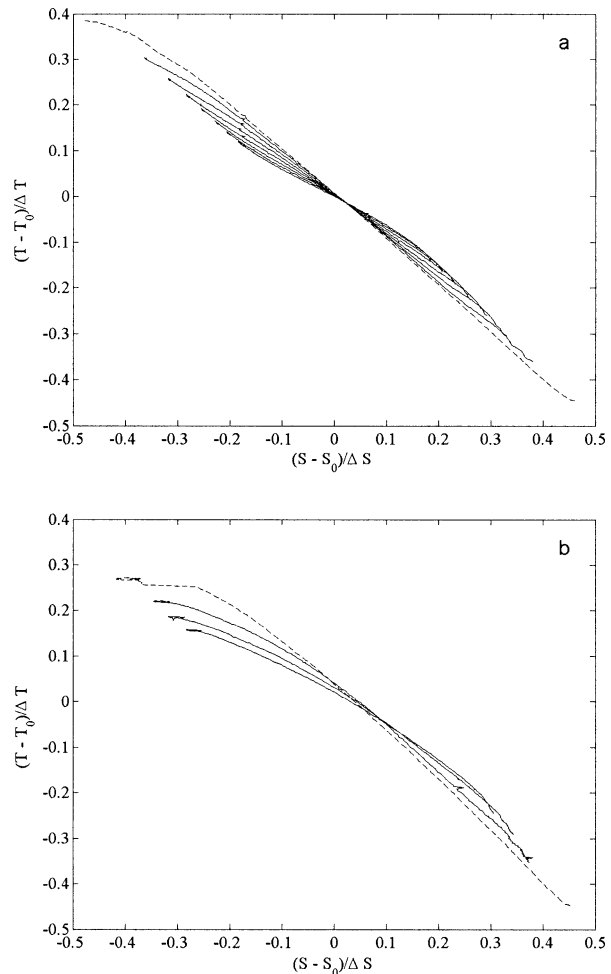


FIG. 4. Typical T – S diagrams: (a) expt 8 and (b) expt 9. The initial profiles are shown as dashed lines. The temperature and salinity differences ΔT and ΔS are computed as the maximum difference in initial profiles, and T_0 and S_0 are the mean temperature and salinity from initial profiles.

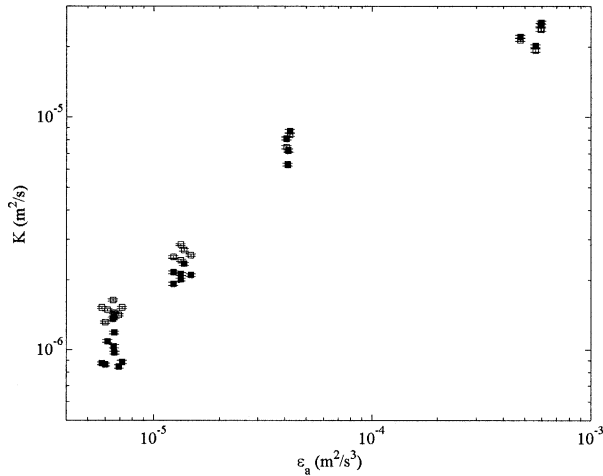


FIG. 5. Eddy diffusivities of temperature and salinity as a function of the average dissipation rate. Filled squares denote K_S and open squares denote K_T . Error bars on the eddy diffusivities reflect measurement uncertainty.

5. Values range from $O(10^{-6})$ to $O(10^{-5})$ $m^2 s^{-1}$ over two decades of dissipation. The eddy diffusivity for temperature varies between 10 and 100 times the molecular diffusivity of temperature, while the eddy diffusivity for salt varies between 1000 and 10^4 times the molecular diffusivity of salt. As the intensity of the stirring increases, both diffusivities increase and they become nearly equal.

Laboratory experiments with temperature-stratified water are subject to some potential artifacts. Because the molecular diffusivity of temperature exceeds that of salt, heat can be preferentially transported into and out of sidewall boundary layers, and a vertical heat flux will result. This effect is analyzed further and shown to be small for the present experiments in the appendix. Another effect is the heating or cooling of the tank water by heat fluxes through the sidewalls. The observed turbulent temperature fluxes, computed with the eddy diffusivities in Fig. 5, vary between 300 and 3000 W for the high-density-ratio experiments and 100 and 1100 W for the low-density-ratio experiments. From the heat loss experiments discussed in section 2, the fluxes through the sidewalls were 0.6%–9% of the observed vertical turbulent heat fluxes; the largest fluxes occurred for the high density ratio experiments. Because the lowest water temperature in the tank was at or above room temperature for all experiments, fluxes through the sidewalls cooled the entire water column.

Barry et al. (2001) recently measured eddy diffusivities as a function of $\varepsilon_a/\nu N^2$ in towed grid experiments with salt-stratified water and a salt-stratified water–glycerol solution. They reported two regimes of behavior: energetic turbulence with high $\varepsilon_a/\nu N^2$ and weak turbulence with low $\varepsilon_a/\nu N^2$. An erroneous factor of the grid solidity in their energy budget rendered the reported values of dissipation a factor of about 2.8 lower than

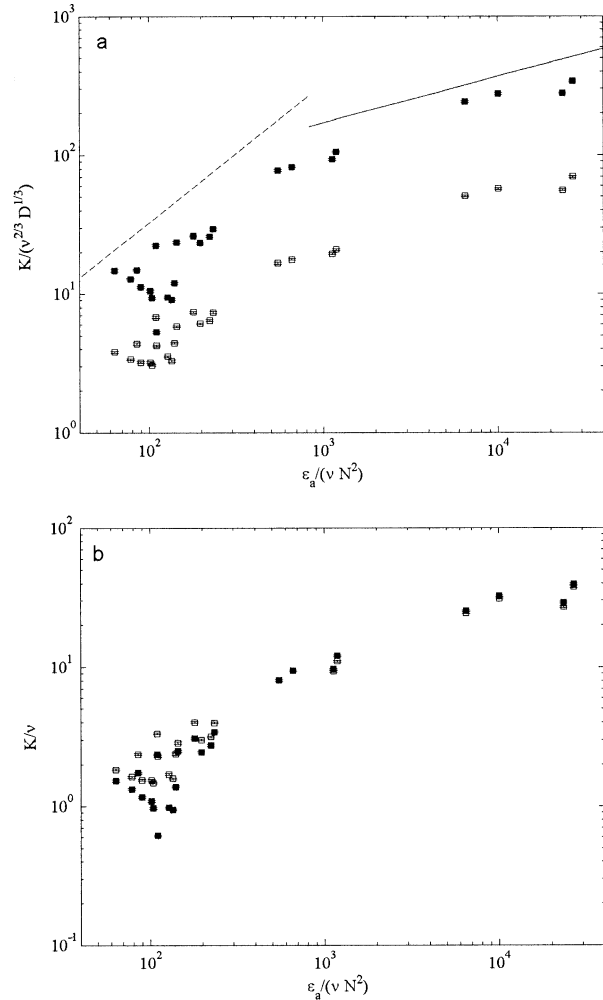


FIG. 6. Dimensionless eddy diffusivities of temperature and salinity: (a) normalization as in Barry et al. (2001); (b) normalization by the kinematic viscosity. Filled squares denote K_S and open squares denote K_T . The viscosity is computed from the mean scalar values from each profile set. In (a), the relationships found by Barry et al. (2001) for the eddy diffusivity of density are shown.

the actual values (G. Ivey 2003, personal communication). If the dissipations are recomputed, the transition between the two regimes occurs at $\varepsilon_a/\nu N^2 \approx 800$. For energetic turbulence, they found that a relationship of the form $K/\nu^{2/3} D^{1/3} \propto (\varepsilon_a/\nu N^2)^{1/3}$ collapsed their eddy diffusivities for density. For weak turbulence, the dependence on $\varepsilon_a/\nu N^2$ was linear, but no data from the water–glycerol solution were available to test Schmidt number effects. In contrast, over the range $200 < \varepsilon_a/\nu N^2 < 10^5$, RK found no measurable effect of the molecular diffusivity on the eddy diffusivities in towed grid experiments with either temperature-stratified or salt-stratified water; thus, normalizing eddy diffusivities by the viscosity collapsed the data fairly well.

Eddy diffusivities for temperature and salinity are normalized with the scaling of Barry et al. (2001) in Fig. 6a and with the kinematic viscosity in Fig. 6b. The

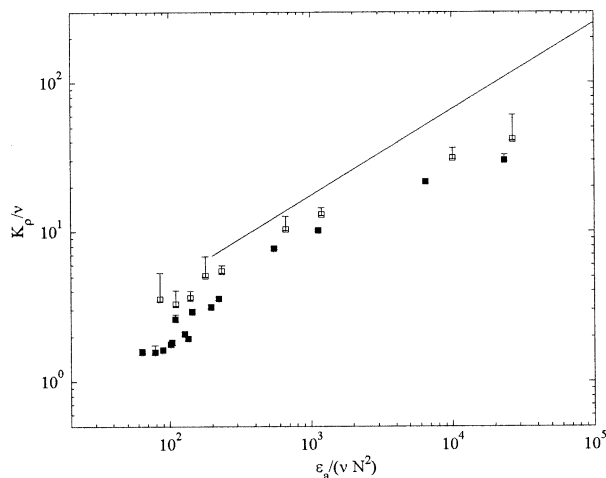


FIG. 7. Dimensionless eddy diffusivity of density. Filled squares have low density ratio, and open squares have high density ratio. The line indicates values from RK over the range $\epsilon_a/\nu N^2$ for which they had both salt- and temperature-stratified cases.

dependence of the present data on $\epsilon_a/\nu N^2$ is consistent with that found by Barry et al. (2001), though the scatter for smaller $\epsilon_a/\nu N^2$ makes quantitative comparison difficult (Fig. 6a). However, normalizing the eddy diffusivities by $\nu^{2/3} D^{1/3}$ fails to collapse the data. Normalizing by the viscosity collapses the eddy diffusivities for $\epsilon_a/\nu N^2 > 300$ (Fig. 6b). For weaker turbulence, the data clouds overlap, but differences between eddy diffusivities of salt and temperature taken from the same profile sets will be shown below to be due to differential diffusion.

Eddy diffusivities for density are shown in Fig. 7. Like the eddy diffusivities for temperature and salinity, K_ρ increases with $\epsilon_a/\nu N^2$; in particular, $K_\rho/\nu \propto (\epsilon_a/\nu N^2)^{0.4}$. The Osborn (1980) relation gives $K_\rho = \Gamma \epsilon_a/\nu N^2$, where the factor Γ is related to the mixing efficiency. If Γ is taken as a constant, as often assumed, then the Osborn (1980) relation predicts a linear dependence between K_ρ/ν and $\epsilon_a/\nu N^2$. The results in Fig. 7 show that for this flow Γ (or the mixing efficiency—see the next subsection) depends on the stratification. The results can also be used to show that the Osborn relation overpredicts K_ρ if Γ is taken as its estimated maximum of 0.2 (Osborn 1980), as Barry et al. (2001) showed for grid turbulence.

The present values of K_ρ agree fairly well with those of RK for low $\epsilon_a/\nu N^2$, but they are a factor of up to 3 lower than their diffusivities at high $\epsilon_a/\nu N^2$. The unsteadiness of towed-grid experiments requires an estimate of the duration of turbulent mixing for calculating eddy diffusivities; uncertainty in the time scale estimates translates to uncertainty in K_ρ . The steadiness of the present experiments eliminates that uncertainty. As in the towed-grid experiments, normalizing by ν collapses the data fairly well for $\epsilon_a/\nu N^2 > 300$, though the data with high density ratio are slightly higher. The small difference for

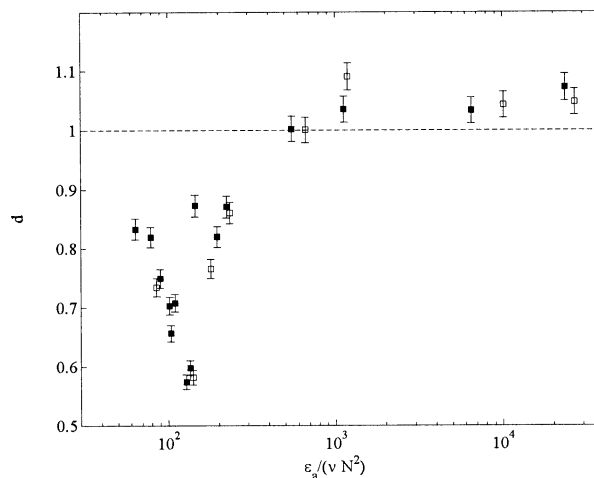


FIG. 8. The diffusivity ratio $d = K_s/K_T$ as a function of $\epsilon_a/\nu N^2$. Filled squares have low density ratio, and open squares have high density ratio.

$\epsilon_a/\nu N^2 > 300$ arises only when the viscosity variations are considered. For $\epsilon_a/\nu N^2 < 300$, the high density ratio and low density ratio data spread further. No such spread appeared in the experiments of RK, though they had only salt-stratified cases for small $\epsilon_a/\nu N^2$.

The diffusivity ratio $d = K_s/K_T$ is plotted against $\epsilon_a/\nu N^2$ in Fig. 8. Above $\epsilon_a/\nu N^2$ of about 300–500, the diffusivity ratio is close to or slightly above unity. For smaller $\epsilon_a/\nu N^2$, the values of d are scattered, but they are well below unity. Thus, these experiments show that differential diffusion occurs for $\epsilon_a/\nu N^2 < 300$ –500. Nash and Moum (2002) found that the diffusivity ratio based on scalar dissipation measured in the ocean over the range $10 < \epsilon/\nu N^2 < 10^5$ yield a mean value of about 0.7, though they could not rule out $d \approx 1$ because of uncertainty in their measurements. Despite differences in stratification and forcing between the present experiments and Turner's (1968) experiments, the values of d compare well, although Turner's results predict that differential diffusion occurs at lower $\epsilon/\nu N^2$.

c. Mixing efficiency

The mixing efficiency is shown as a function of the Richardson number $Ri_\tau = Fr_\tau^{-2}$ and initial density ratio in Fig. 9. The magnitude of the efficiency and the dependence on the Richardson number agree with observations from previous experiments. Over the range of Richardson number considered the efficiencies are less than 4%. Efficiencies from several experiments compiled by Linden (1979) reach a maximum of 25%, but the efficiencies compiled from several towed grid experiments are less than about 6% (RK). Trends with Richardson number are also qualitatively similar; at small Richardson number the efficiency is small, and it increases as Ri_τ increases, as in towed grid experiments.

Despite these similarities, the results of the present

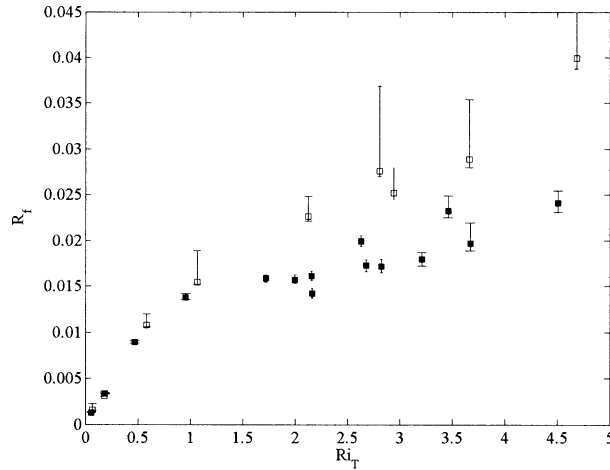


FIG. 9. Mixing efficiency as a function of the Richardson number. Filled squares have low density ratio, and open squares have high density ratio.

experiments differ from those of previous experiments in important ways. For $Ri_T < 1$ mixing efficiencies in high and low density ratio experiments agree well. However, for $Ri_T > 1$ mixing efficiencies at high density ratio exceed those at low density ratio by about 50%. In contrast, RK found that efficiencies in a temperature-stratified fluid agreed with efficiencies in a salt-stratified fluid within the experimental uncertainty over a large range of a Richardson number based on bulk quantities. As the discussion of eddy diffusivities suggests, the forcing in the experiments of RK was too energetic, or $\epsilon_a/\nu N^2$ was too large, for effects of the molecular diffusivity to appear.

In towed-grid experiments with either temperature or salinity stratification, the data collapse to a single efficiency-Richardson number curve (RK) that follows the scaling of Britter (1985). In the present experiments, the efficiency for low density ratio approaches a constant—or at least increases less steeply—as the Richardson number increases, while the efficiency for high density ratio continues to increase for $Ri_T > 1$. Because heat transport is greater than salinity transport at high Richardson numbers, the potential energy change and thus the mixing efficiency are greater when more of the density gradient is due to temperature—that is, when the density ratio is larger. Similar behavior is observed in efficiencies computed from Turner's (1968) laboratory data; as the density ratio decreases the efficiency increases less steeply and can even decrease with increasing Ri_T (Jackson and Rehmann 2003). Quantitatively comparing these calculations with the present experimental data is not possible because of differences between the mixing mechanisms.

The results in Fig. 9 show that differential diffusion can affect the mixing efficiency significantly. Linden's (1979) compilation of measurements from various laboratory experiments shows that the mixing

efficiency depends on the stratification strength, measured by a Richardson number, and the process generating the turbulence. A similar conclusion holds for efficiencies based on the buoyancy flux (Ivey and Imberger 1991). In the present experiments, the efficiency depends strongly on the stratification strength, but above $Ri_T > 1$ effects of differential diffusion are comparable. For example, over the range $1 < Ri_T < 5$, R_f increases by a factor of 1.5 for the case with $R_p \approx 0.25$. This increase is comparable to the difference between the high and low density ratio cases for a Richardson number of 5.

4. Summary

We performed laboratory experiments to determine the conditions under which differential diffusion occurs and evaluate its effect on the mixing efficiency. Diffusively stable profiles of temperature and salinity were stirred steadily by horizontally oscillating vertical rods. The two-component stratification ensures that both scalars experience the same stratification and forcing, or Richardson and Reynolds numbers. Temperature and salinity profiles were obtained with a temperature-conductivity probe, and the work done by the rods on the water was measured with a force transducer. The eddy diffusivities K_T and K_S were estimated by fitting theoretical solutions of diffusion equations to the measured profiles for temperature and salinity, and the mixing efficiency was computed as the ratio of the potential energy change during a stirring interval to the work done in that interval. The average dissipation rate ϵ_a was computed from the work measurements and an integrated energy budget.

We observed differential diffusion and identified conditions for its occurrence. Here T - S diagrams qualitatively show the effects of differential diffusion. One can determine whether the diffusivity ratio $d = K_S/K_T$ is larger or smaller between two cases by comparing T - S diagrams, but care must be taken to compare equal time intervals made dimensionless by H^2/K_T . Differential diffusion occurred for $\epsilon_a/\nu N^2 < 300$ -500 or for $Ri_T > 1$. The diffusivity ratio varied between 0.5 and 1 in the range $50 < \epsilon_a/\nu N^2 < 500$. For similar values of $\epsilon_a/\nu N^2$ Barry et al. (2001) noted a change in the behavior of the turbulence, though they did not have data to evaluate Schmidt number effects. In the present experiments, eddy diffusivities of temperature, salinity, and density collapsed well when normalized by the kinematic viscosity for large $\epsilon_a/\nu N^2$. The data did not collapse as well when differential diffusion occurred.

The experiments also illustrate the effect of differential diffusion on the mixing efficiency. When differential diffusion occurs, the density ratio will be important. If $K_T > K_S$, then the mixing efficiency will be greater in cases in which more of the stratification is caused by temperature. We measured mixing efficiencies for cases with low density ratio ($R_p \approx 0.25$) and

high density ratio ($R_\rho \approx 5$). In both cases, the efficiency increased from 0 to 1.5% as the Richardson number Ri_T increased from 0 to 1. However, for $Ri_T > 1$, the efficiency for the high-density-ratio case exceeded that for the low-density-ratio case and increased more rapidly. The measurements show that effects of differential diffusion on the mixing efficiency can be significant.

Acknowledgments. We thank Barry Ruddick and Ann Gargett for pointing out the problem of transport in the sidewall boundary layer, which they discovered in their past experiments. The first subsection of the appendix is based on calculations that Dr. Ruddick sent to us. This work was supported by the National Science Foundation under Grant OCE 99-77208. Any opinions, findings, and conclusions or recommendations expressed in this material are those of the authors and do not necessarily reflect the views of the National Science Foundation.

APPENDIX

Transport in Sidewall Boundary Layers

Besides differential diffusion, a potential reason for the heat flux to exceed the salt flux in the present experiments is transport of heat via molecular diffusion into and out of the sidewall boundary layer. Consider a bounded flow driven in a manner that creates a vertical oscillation of the isopycnals (Fig. A1). Internal waves in a temperature-stratified tank would be one such flow. At the walls of the tank, boundary layers will develop. As in Stokes's second problem (e.g., Panton 1984, section 11.2), quantities in the boundary layer lag the outer flow. Thus, when a wave trough forces the isotherms to drop near the wall, the temperature will increase away from the wall, and heat will diffuse into the boundary layer. Likewise, when the isotherms rise in the outer flow, the temperature will decrease away from the wall, and heat will diffuse out of the boundary layer. This mechanism can transfer heat at much higher rates than salt due to the difference in the molecular diffusivities of the two scalars. We first compute the sidewall boundary layer (SBL) flux for forcing at a single frequency and then extend the results for a homogeneous, turbulent flow.

a. Monochromatic forcing

We first consider the case of a flow oscillating at a frequency ω in a semi-infinite fluid and compute the

vertical heat flux from the product of the temperature and vertical velocity w . If the boundary layer is thin and products of fluctuations are small, the momentum equation is

$$\frac{\partial w}{\partial t} = -\frac{1}{\rho_0} \frac{\partial p}{\partial z} + \nu \frac{\partial^2 w}{\partial x^2}, \quad (\text{A1})$$

where $\partial p/\partial z = \rho_0 w_0 \omega \sin(\omega t)$ represents the oscillatory pressure gradient necessary to drive the flow and w_0 is the amplitude of the vertical velocity. The boundary conditions are

$$w(0) = 0, \quad w(\infty) = w_0 \cos(\omega t)$$

satisfying no slip and the oscillatory outer flow, respectively. This problem is equivalent to a wall oscillating next to stationary fluid (Panton 1984, section 11.2). In complex form, the solution is

$$w(x, t) = w_0 e^{i\omega t} [1 - e^{-(1+i)x/\delta}], \quad (\text{A2})$$

where $\delta = \sqrt{2\nu/\omega}$.

Under the assumptions used for the momentum equation, [Eq. (A1)], the governing equation for temperature is

$$\frac{\partial T}{\partial t} + w \frac{d\bar{T}}{dz} = D \frac{\partial^2 T}{\partial x^2}. \quad (\text{A3})$$

At $x = 0$, the heat flux is assumed to be zero, and far from the wall the temperature is that for internal waves:

$$\begin{aligned} \frac{\partial T}{\partial x} &= 0 && \text{at } x = 0 \\ T &= -\frac{w_0 (d\bar{T}/dz)}{i\omega} e^{i\omega t} && \text{as } x \rightarrow \infty. \end{aligned}$$

The solution for the temperature is then

$$T = \frac{i w_0 (d\bar{T}/dz)}{\omega} e^{i\omega t} \left[1 + \frac{\text{Pr}^{1/2} e^{-(1+i)x/\delta_T} - \text{Pr} e^{-(1+i)x/\delta}}{\text{Pr} - 1} \right], \quad (\text{A4})$$

where the Prandtl number $\text{Pr} = \nu/D$ and $\delta_T = \sqrt{2D/\omega} = \delta/\text{Pr}^{1/2}$.

The heat flux is computed from the product of w and T . The real parts of Eq. (A2) and Eq. (A4) are

$$w(x, t) = w_0 \left[\cos(\omega t) - e^{-x/\delta} \cos\left(\frac{x}{\delta} - \omega t\right) \right] \quad (\text{A5})$$

$$T(x, t) = -\frac{w_0 d\bar{T}}{\omega dz} \left[\sin(\omega t) + \frac{\text{Pr} e^{-x/\delta} \sin\left(\frac{x}{\delta} - \omega t\right) - \sqrt{\text{Pr}} e^{-x/\delta} \sin\left(\frac{x}{\delta_T} - \omega t\right)}{\text{Pr} - 1} \right]. \quad (\text{A6})$$

TABLE A1. Estimates of the effect of the sidewall boundary layer on vertical heat transport. Values of the sidewall boundary layer diffusivity K_{SBL} and flux ratio F_r are computed from Eqs. (A13) and (A14) for $N = 0.3$ rad/s, $G = 66$, $F = 0.52$, and $\gamma = 0.12$, which are typical of our most strongly stratified cases. The diffusivities are computed with $\Lambda = B = 0.4$ m, while in computing the total SBL flux, the appropriate value of Λ is used.

n	Buoyancy scaling		Inertial scaling	
	K_{SBL} ($\text{m}^2 \text{s}^{-1}$)	F_r (%)	K_{SBL} ($\text{m}^2 \text{s}^{-1}$)	F_r (%)
0	2×10^{-9}	0.4	2×10^{-9}	0.4
1	6×10^{-9}	1.2	7×10^{-9}	1.3
2	2×10^{-8}	4.6	3×10^{-8}	5.6

The SBL flux can be found by averaging the product of w and T over one period and the dimension Λ of the tank:

$$\begin{aligned}
 F_{\text{SBL}} &= \frac{\omega}{2\pi\Lambda} \int_0^\Lambda \int_0^{2\pi/\omega} wT \, dt \, dx \\
 &\approx \frac{\omega}{2\pi\Lambda} \int_0^\infty \int_0^{2\pi/\omega} wT \, dt \, dx \\
 &= -\frac{w_0^2 \delta}{\omega\Lambda} f(\text{Pr}) \frac{d\bar{T}}{dz}, \quad (\text{A7})
 \end{aligned}$$

where

$$f(\text{Pr}) = \frac{1}{4} \frac{\text{Pr} - \text{Pr}^{1/2}}{\text{Pr}^2 - 1}.$$

The approximation in Eq. (A7) is valid when $\Lambda/\delta \gg 1$. The diffusivity due to the SBL is

$$K_{\text{SBL}} = f(\text{Pr}) \frac{w_0^2 \delta}{\omega\Lambda}. \quad (\text{A8})$$

Equations (A7) and (A8) apply for a single wall; in applying the results of the next section to our experiments, we add the contributions from all of the walls.

The results of this section show that the diffusivity of salt due to the SBL is small compared to the SBL diffusivity of temperature. Evaluating Eq. (A8) for heated water ($\text{Pr} = 7$) and for salt water ($\text{Pr} = 700$) yields

$$\frac{K_{\text{S,SBL}}}{K_{\text{T,SBL}}} = 0.015.$$

Thus, if the SBL heat flux is comparable to the vertical heat flux being studied, the SBL flux would not only change the magnitude of the observed diffusivity but also appear as differential diffusion.

b. Turbulent forcing

The above analysis presents the case of outer flow consisting of an oscillatory motion at one frequency. We now consider a turbulent outer flow, in which w_0 can vary as a function of ω , and write

$$w_0 = w_0(\omega) = \sqrt{2E_{\text{ww}}(\omega)d\omega},$$

where $E_{\text{ww}}(\omega)$ is the spectrum of vertical velocity. We assume that Eqs. (A1) and (A3) still hold for this turbulent flow. A similar set of equations has been used to study weak turbulence in a stratified fluid (Deissler 1962), the final period of decay (Pearson and Linden 1983), and rapid distortion of strongly stratified turbulence (e.g., Hanazaki and Hunt 1996). In particular, Hanazaki and Hunt (1996) showed that linear processes explain much of the behavior observed in grid turbulence experiments (e.g., Lienhard and Van Atta 1990). Because our experiments show that differential diffusion occurs for weak turbulence in a strongly stratified fluid (i.e., small $\varepsilon/\nu N^2$, or large Ri_T), a linear model should provide a reasonable first approximation for the effects of the sidewalls. Then, from Eq. (A7) the contribution to the SBL flux from frequencies in a band of width $d\omega$ centered on frequency ω can be written

$$\begin{aligned}
 df_{\text{SBL}} &= \frac{1}{\Lambda} \int_0^\infty \left(\frac{\omega}{2\pi} \int_0^{2\pi/\omega} wT \, dt \right) dx \\
 &= -\frac{2E_{\text{ww}}(\omega)d\omega}{\omega} \left(\frac{\delta}{\Lambda} \right) \frac{d\bar{T}}{dz} f(\text{Pr})
 \end{aligned}$$

so that, since $\delta = \sqrt{2\nu/\omega}$, the total flux is

$$f_{\text{SBL}} = -2^{3/2} f(\text{Pr}) \frac{\nu^{1/2}}{\Lambda} \frac{d\bar{T}}{dz} \int_0^\infty \omega^{-3/2} E_{\text{ww}}(\omega) \, d\omega. \quad (\text{A9})$$

To proceed, the velocity spectrum must be defined. In grid turbulence experiments (Itsweire et al. 1986; Lienhard and Van Atta 1990), the vertical velocity spectrum rolls off sharply at high frequencies (or wavenumbers) and remains approximately constant at intermediate frequencies. At low wavenumbers the spectrum either stays constant or rises with decreasing wavenumber k due to internal waves; that is, spectra follow k^{-n} , where $0 < n < 2$. Thus, we model the spectrum as constant between the buoyancy frequency and a high frequency cutoff, allow for a low frequency rise, and use the normalization for the Eulerian time spectrum (Tennekes and Lumley 1989, section 8.5):

$$\frac{E_{\text{ww}}(\omega)}{u_\kappa^2(\eta/u)} = \begin{cases} E_0 \left(\frac{\omega}{N} \right)^{-n}, & \gamma N < \omega < N \\ E_0, & N < \omega < \frac{u}{\eta} \\ 0, & \omega > \frac{u}{\eta}, \end{cases} \quad (\text{A10})$$

where $u^2 = q^2/3$, $q^2/2$ is the turbulent kinetic energy, and $\eta = (\nu^3/\varepsilon)^{1/4}$ and $u_\kappa = (\nu\varepsilon)^{1/4}$ are the Kolmogorov length and velocity scales, respectively. The spectrum is sketched in Fig. A2. The high-frequency cutoff is set from the measurements of Lienhard and Van Atta (1990), which show that the frequency spectra roll off at $\omega \sim u/\eta$. The lowest frequency is set with the parameter γ . Barrett (1989) observed long internal waves

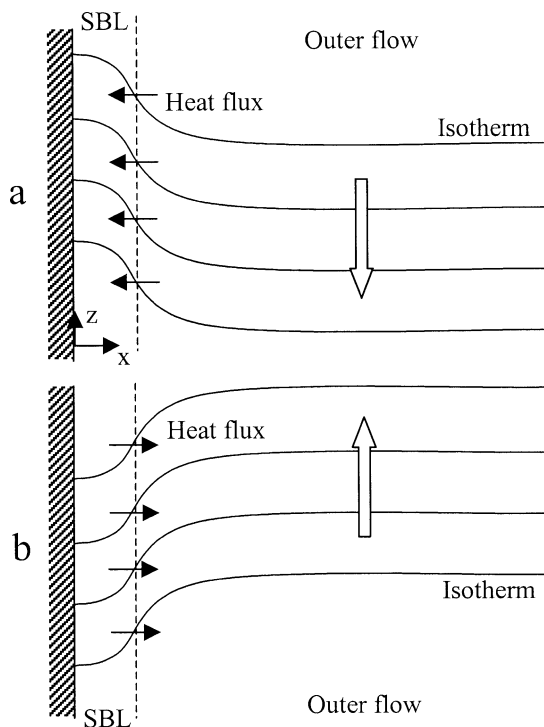


FIG. A1. Schematic showing the mechanism for diffusion of heat into and out of the sidewall boundary layer set up by an oscillating outer flow near a stationary boundary: (a) dropping of the isotherms and flux into the boundary layer; (b) rising of the isotherms and diffusion out of the boundary layer.

after the decay of turbulence in grid towing experiments; the dominant mode was the (1, 0, 2) mode. For our experiments, the (1, 0, 2) mode corresponds to $\gamma = 0.12$. From grid turbulence experiments, the spectral slope is between -2 and 0 , giving $0 < n < 2$.

The constant E_0 and velocity u can be related with the vertical velocity variance, or the integral of the spectrum:

$$u^2 \cong c\bar{w}^2 = 2c \int_0^\infty E_{ww}(\omega) d\omega,$$

where c is a coefficient that depends on the isotropy of the turbulence. Solving for E_0 yields

$$E_0 = \frac{1}{2c} \left(\frac{u}{u_k} \right)^2 \left(1 + a_1 \frac{N\eta}{u} \right)^{-1}, \quad (\text{A11})$$

where $a_1 = [\gamma^{-(n-1)} - 1]/(n-1) - 1$ for $n \neq 1$ and $a_1 = \ln(1/\gamma) - 1$ for $n = 1$. The diffusivity through SBL, calculated with Eqs. (A9)–(A11), is

$$K_{\text{SBL}} = \frac{2^{3/2}}{c} f(\text{Pr}) \left(\frac{\nu}{N\Lambda^2} \right)^{1/2} u\eta \left[\frac{a_2 - \left(\frac{N\eta}{u} \right)^{1/2}}{1 + a_1 \frac{N\eta}{u}} \right], \quad (\text{A12})$$

where $a_2 = 1 + [\gamma^{-(n+1/2)} - 1]/(2n+1)$.

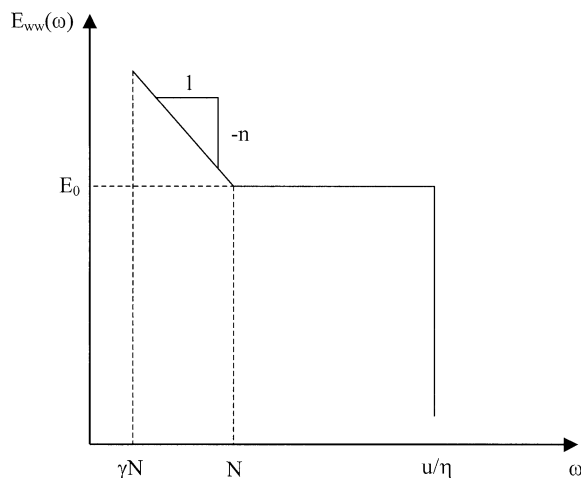


FIG. A2. Vertical velocity spectrum assumed to model turbulent forcing.

Because velocities were not measured in our experiments, we use two estimates of the velocity u . Inertial scaling gives $u \approx c_I(\varepsilon L_T)^{1/3}$, while buoyancy scaling gives $u \approx c_O(\varepsilon/N)^{1/2}$, where c_I and c_O are coefficients and L_T is the length scale of the large eddies. From Eq. (A12) the diffusivity is

$$\frac{K_{\text{SBL}}}{\nu} = 2^{3/2} \frac{c_I}{c} f(\text{Pr}) \left(\frac{\nu}{N\Lambda^2} \right)^{1/2} \frac{G^{1/4}}{F^{1/2}} \left(\frac{a_2 - c_I^{-1/2} F^{1/4} G^{-3/8}}{1 + a_1 c_I^{-1} F^{1/2} G^{-3/4}} \right) \quad (\text{A13})$$

for inertial scaling and

$$\frac{K_{\text{SBL}}}{\nu} = 2^{3/2} \frac{c_O}{c} f(\text{Pr}) \left(\frac{\nu}{N\Lambda^2} \right)^{1/2} G^{1/4} \left(\frac{a_2 - c_O^{-1/2} G^{-3/8}}{1 + a_1 c_O^{-1} G^{-3/4}} \right) \quad (\text{A14})$$

for buoyancy scaling, where $G = \varepsilon/\nu N^2$ and $F = \varepsilon^{1/3}/NL_T^{2/3}$ is the turbulent Froude number of Ivey and Imberger (1991).

Equations (A13) and (A14) can be used to estimate the significance of SBL fluxes in our experiments. Ivey and Imberger (1991) find $c_I = 2$, and average values computed from the data of Itsweire et al. (1986) yield $c = 1.3$ and $c_O = 1.3$. Table A1 lists values of K_{SBL} computed with parameter values typical of our most strongly stratified cases and three values of the spectral exponent n . All values of the sidewall boundary layer diffusivity are less than molecular diffusivity of temperature. Perhaps a better comparison is between the total SBL flux ΣF_{SBL} over the four tank walls and the observed turbulent flux $F_T = -K_T BL(d\bar{T}/dz)$. The ratio of these fluxes, $F_r = \Sigma F_{\text{SBL}}/F_T$, is also shown in Table A1.

For our experiments the effect of the sidewall boundary layer is small. The estimated SBL diffusivities are quite small in comparison with the observed eddy dif-

fusivities; all are at least a factor of 30 smaller than the smallest value of K_T . As $\varepsilon/\nu N^2$ increases, K_T will be even larger than K_{SBL} since Eq. (A14) shows that $K_{SBL} \propto (\varepsilon/\nu N^2)^{0.3}$, while K_T increases faster (Fig. 6). Also, all of the estimates of the flux ratio are less than 6%. Essentially all of the flux comes from the internal wave part of the spectrum; if the waves were eliminated (i.e., $\gamma = 1$), the flux ratio would be 0.1%. For this reason, we expect the estimates in Table A1 to be conservative. Internal waves should have relatively little energy in our experiments because our stirring mechanism has no horizontal bars, unlike the grids in the experiments of Itsweire et al. (1986) and Lienhard and Van Atta (1990). Analysis of temperature fluctuations during stirring shows flat spectra for frequencies smaller than N . A low-frequency rise, corresponding to long internal waves, does occur when the stirring is stopped, but the energy is 10 times as small as that during stirring. An analysis similar to that above but neglecting the turbulence portion of the spectrum shows that at this energy level the SBL fluxes due to waves in the 12-min waiting period are less than 0.4% of the fluxes due to turbulence.

REFERENCES

- Altman, D. B., and A. E. Gargett, 1990: Differential property transport due to incomplete mixing in a stratified fluid. *Stratified Flows*, E. J. List and G. H. Jirka, Eds., American Society of Civil Engineers, 454–460.
- Barrett, T. K., 1989: Nonintrusive optical measurements of turbulence and mixing in a stably stratified fluid. Ph.D. thesis, University of California, San Diego, 242 pp.
- , and C. W. Van Atta, 1991: Experiments on the inhibition of mixing in stably stratified decaying turbulence using laser Doppler anemometry and laser-induced fluorescence. *Phys. Fluids A*, **3**, 1321–1332.
- Barry, M. E., G. N. Ivey, K. B. Winters, and J. Imberger, 2001: Measurements of diapycnal diffusivities in stratified fluids. *J. Fluid Mech.*, **442**, 267–291.
- Britter, R. E., 1985: Diffusion and decay in stably-stratified turbulent flows. *Turbulence and Diffusion in Stable Environments*, J. C. R. Hunt, Ed., Clarendon, 3–13.
- Deissler, R. G., 1962: Turbulence in the presence of a vertical body force and temperature gradient. *J. Geophys. Res.*, **67**, 3049–3062.
- Fortuin, J., 1960: Theory and application of two supplementary methods of constructing density gradient columns. *J. Polym. Sci.*, **44**, 505–515.
- Gargett, A. E., 2003: Differential diffusion: An oceanographic primer. *Progress in Oceanography*, Vol. 56, Pergamon, in press.
- , and G. Holloway, 1992: Sensitivity of the GFDL ocean model to different diffusivities of heat and salt. *J. Phys. Oceanogr.*, **22**, 1158–1177.
- , and B. Ferron, 1996: The effects of differential vertical diffusion of T and S in a box model of thermohaline circulation. *J. Mar. Res.*, **54**, 827–866.
- Hanazaki, H., and J. C. R. Hunt, 1996: Linear processes in unsteady stably stratified turbulence. *J. Fluid Mech.*, **318**, 303–337.
- Head, M. J., 1983: The use of miniature four-electrode conductivity probes for high resolution measurement of turbulent density or temperature variations in salt-stratified water flows. Ph.D. thesis, University California, San Diego, 211 pp.
- Holford, J. M., and P. F. Linden, 1999: Turbulent mixing in a stratified fluid. *Dyn. Atmos. Oceans*, **30**, 173–198.
- Imberger, J., and G. N. Ivey, 1991: On the nature of turbulence in a stratified fluid. Part II: Application to lakes. *J. Phys. Oceanogr.*, **21**, 659–680.
- Itsweire, E. C., K. N. Helland, and C. W. Van Atta, 1986: The evolution of grid-generated turbulence in a stably stratified fluid. *J. Fluid Mech.*, **162**, 299–338.
- Ivey, G. N., and J. Imberger, 1991: On the nature of turbulence in a stratified fluid. Part I: The energetics of mixing. *J. Phys. Oceanogr.*, **21**, 650–658.
- Jackson, P. R., and C. R. Rehmann, 2003: Kinematic effects of differential transport on mixing efficiency in a diffusively stable, turbulent flow. *J. Phys. Oceanogr.*, **33**, 299–304.
- Lienhard, J. H., and C. W. Van Atta, 1990: The decay of turbulence in a thermally stratified flow. *J. Fluid Mech.*, **210**, 57–112.
- Linden, P. F., 1979: Mixing in stratified fluids. *Geophys. Astrophys. Fluid Dyn.*, **13**, 3–23.
- , 1980: Mixing across a density interface produced by grid turbulence. *J. Fluid Mech.*, **100**, 691–703.
- Merryfield, W. J., G. Holloway, and A. E. Gargett, 1998: Differential vertical transport of heat and salt by weak stratified turbulence. *Geophys. Res. Lett.*, **25**, 2773–2776.
- , —, and —, 1999: A global ocean model with double-diffusive mixing. *J. Phys. Oceanogr.*, **29**, 1124–1142.
- Muñoz, D., and F. Zangrando, 1986: Mixing in a double-diffusive, partially stratified fluid. Solar Energy Research Institute Rep. SERI/TR-252-2942, 121 pp.
- Nagata, K., and S. Komori, 2001: The difference in turbulence diffusion between active and passive scalars in stable thermal stratification. *J. Fluid Mech.*, **430**, 361–380.
- Nash, J. D., and J. N. Moum, 2002: Microstructure estimates of turbulent salinity flux and the dissipation spectrum of salinity. *J. Phys. Oceanogr.*, **32**, 2312–2333.
- Oakey, N. S., 1982: Determination of the rate of dissipation of turbulent energy from simultaneous temperature and velocity shear microstructure measurements. *J. Phys. Oceanogr.*, **12**, 256–271.
- Osborn, T., 1980: Estimates of the local rate of vertical diffusion from dissipation measurements. *J. Phys. Oceanogr.*, **10**, 83–89.
- , and C. S. Cox, 1972: Oceanic fine structure. *Geophys. Fluid Dyn.*, **3**, 321–345.
- Panton, R. L., 1984: *Incompressible Flow*. Wiley, 780 pp.
- Park, Y.-G., J. A. Whitehead, and A. Gnanadeskian, 1994: Turbulent mixing in stratified fluids: Layer formation and energetics. *J. Fluid Mech.*, **279**, 279–311.
- Pearson, H. J., and P. F. Linden, 1983: The final stage of decay of turbulence in a stably stratified fluid. *J. Fluid Mech.*, **134**, 195–203.
- Rottman, J. W., and R. E. Britter, 1986: The mixing efficiency and decay of grid-generated turbulence in stably-stratified fluids. *Proc. Ninth Australasian Fluid Mechanics Conf.*, Auckland, New Zealand, University of Auckland, 218–221.
- Ruddick, B. R., T. J. McDougall, and J. S. Turner, 1989: The formation of layers in a uniformly stirred density gradient. *Deep-Sea Res.*, **36**, 597–609.
- Sumer, B. M., and J. Fredsøe, 1997: *Hydrodynamics around Cylindrical Structures*. World Scientific, 530 pp.
- Tennekes, H., and J. L. Lumley, 1989: *A First Course in Turbulence*. The MIT Press, 300 pp.
- Turner, J. S., 1968: The influence of molecular diffusivity on turbulent entrainment across a density interface. *J. Fluid Mech.*, **33**, 639–656.